

# Globally rising soil heterotrophic respiration over recent decades

Ben Bond-Lamberty<sup>1\*</sup>, Vanessa L. Bailey<sup>2</sup>, Min Chen<sup>1</sup>, Christopher M. Gough<sup>3</sup> & Rodrigo Vargas<sup>4</sup>

**Global soils store at least twice as much carbon as Earth's atmosphere<sup>1,2</sup>. The global soil-to-atmosphere (or total soil respiration,  $R_S$ ) carbon dioxide (CO<sub>2</sub>) flux is increasing<sup>3,4</sup>, but the degree to which climate change will stimulate carbon losses from soils as a result of heterotrophic respiration ( $R_H$ ) remains highly uncertain<sup>5–8</sup>. Here we use an updated global soil respiration database<sup>9</sup> to show that the observed soil surface  $R_H:R_S$  ratio increased significantly, from 0.54 to 0.63, between 1990 and 2014 ( $P=0.009$ ). Three additional lines of evidence provide support for this finding. By analysing two separate global gross primary production datasets<sup>10,11</sup>, we find that the ratios of both  $R_H$  and  $R_S$  to gross primary production have increased over time. Similarly, significant increases in  $R_H$  are observed against the longest available solar-induced chlorophyll fluorescence global dataset, as well as gross primary production computed by an ensemble of global land models. We also show that the ratio of night-time net ecosystem exchange to gross primary production is rising across the FLUXNET2015<sup>12</sup> dataset. All trends are robust to sampling variability in ecosystem type, disturbance, methodology, CO<sub>2</sub> fertilization effects and mean climate. Taken together, our findings provide observational evidence that global  $R_H$  is rising, probably in response to environmental changes, consistent with meta-analyses<sup>13–16</sup> and long-term experiments<sup>17</sup>. This suggests that climate-driven losses of soil carbon are currently occurring across many ecosystems, with a detectable and sustained trend emerging at the global scale.**

The sensitivity of  $R_H$  to ongoing changes in temperature, precipitation and organic matter input to the soil system remains highly uncertain. Because of the large stocks of global soil organic carbon content (SOC) and quickly changing climatic conditions, this uncertainty has large implications for predicting future dynamics of Earth's climate system and carbon (C) cycle<sup>5</sup>. But because  $R_H$  observations are infrequently performed, necessarily small-scale and highly variable, it is difficult to detect and attribute annual-to-decadal changes at larger spatial scales.

One way to quantify and interpret shifts in the flux of C from SOC is to examine the changing ratios between  $R_H$  and other parts of the C cycle. For example, widespread increases over time in the ratio of  $R_H$  to the larger  $R_S$  flux, a ratio which typically varies in a predictable manner<sup>18</sup>, would suggest that  $R_H$  is rising. Quantifying this change would provide new constraints on whether greater mineralization of SOC is occurring, and the degree to which increased inputs by enhanced gross primary production (GPP) are affecting  $R_H$ <sup>8,19</sup>. We used a global soil respiration database (SRDB)<sup>9</sup>, expanded and updated to include studies reporting data through 2014, to test these possibilities.

The mean  $R_H:R_S$  ratio observed in SRDB has risen over time, from  $0.54 \pm 0.18$  in 1990–1998 to  $0.63 \pm 0.16$  in 2007–2014 (Fig. 1). This change is significant ( $P=0.009$ ,  $n=318$ ) when ecosystem mean annual temperature (MAT) and mean annual precipitation (MAP) are controlled for in a linear model (Table 1, Extended Data Table 1, Extended Data Fig. 1). This trend in the  $R_H:R_S$  ratio was not induced by a site

selection bias, as this model also controls for the possibility of researchers sampling more disturbed sites, sites with varying land cover or SOC stocks, and using different methods to partition  $R_H$  from  $R_S$ . The SRDB covers most of the global climate space (from  $-13.2^{\circ}\text{C}$  to  $27.9^{\circ}\text{C}$  MAT, and from 63 mm to 4,563 mm MAP; Extended Data Fig. 2); examining climate controls<sup>20</sup> on  $R_H$ , both MAP ( $P<0.001$ , exerting a positive effect), and potential evapotranspiration ( $P=0.006$ ) had the strongest effects on annual  $R_H$ , with disturbance and temperature exerting complex interactive effects.

A rising  $R_H:R_S$  ratio could be due to rising SOC losses and thus a climate feedback, and/or increasing GPP rates enhancing detritus inputs and thus counterbalancing C losses from SOC. To distinguish these possibilities, we examined the ratio of all soil-derived respiration fluxes to GPP<sup>21</sup>, the ultimate source of both the autotrophic and heterotrophic soil surface CO<sub>2</sub> fluxes. We note that the more relevant ratio to study is that of  $R_H$  to net primary production (NPP) rather than to GPP,

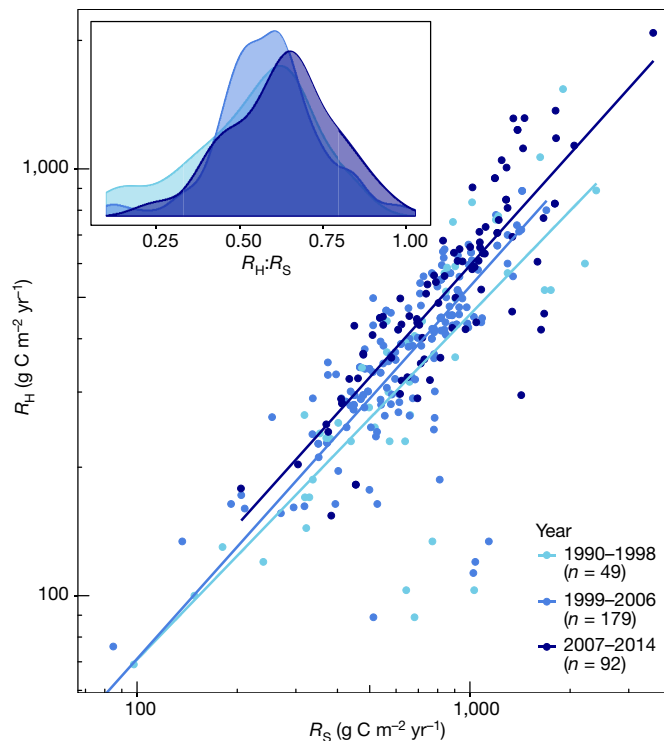


**Fig. 1 | Changes in  $R_H:R_S$  over time.** Data are drawn from unmanaged, unmanipulated ecosystems in a global soil respiration database<sup>9</sup>, binned into 8–9 year groups (this binning is for display only, and was not part of the statistical analysis summarized in Table 1), and shown with linear regression lines; for clarity, one extremely low value is not shown. Note logarithmic axes. Inset, changes in  $R_H:R_S$  density distribution over time. See also Extended Data Table 1.

<sup>1</sup>Pacific Northwest National Laboratory, Joint Global Change Research Institute at the University of Maryland–College Park, College Park, MD, USA. <sup>2</sup>Biological Sciences Division, Pacific Northwest National Laboratory, Richland, WA, USA. <sup>3</sup>Department of Biology, Virginia Commonwealth University, Richmond, VA, USA. <sup>4</sup>Department of Plant and Soil Sciences, University of Delaware, Newark, DE, USA. \*e-mail: bondlamberty@pnnl.gov

**Table 1 | Effects in linear model of how  $R_H:R_S$  changes over time**

Effect	Degrees of freedom	Sum of squares	Mean sum of squares	F	P
Year	1	0.151	0.159	6.972	0.009
Disturbance	1	0.018	0.018	0.826	0.364
Partitioning method	10	0.363	0.036	1.677	0.086
MAT	1	0.439	0.439	20.293	<0.001
MAP	1	0.005	0.005	0.238	0.626
SOC	1	0.408	0.408	18.877	<0.001
Year * Method	7	0.432	0.062	2.853	0.007
MAT * MAP	1	0.075	0.075	3.460	0.064
Year * SOC	1	0.058	0.058	2.656	0.104
Residuals	293	6.339	0.022		

This table summarizes the statistically significant effects in the linear model examining how  $R_H:R_S$  changes over time. Effects tested include year of observation, disturbance (ecosystem coded as aggrading versus mature), method used to partition  $R_H$  from  $R_S$ , land cover (deciduous forest, evergreen forest, grassland, savannah, other), MAT, MAP and SOC. Terms that were not significant in the final model do not appear in the table. An asterisk denotes an effect interaction.

but global NPP estimates are subject to more uncertain assumptions. If increased SOC mineralization rates are raising  $R_H$ , one would expect both  $R_H$  and the total surface efflux  $R_S$  to rise relative to GPP.

The available data support this expectation as both  $R_H$  (the variable of primary interest, but for which far fewer measurements are available) and  $R_S$  (which incorporates both  $R_H$  and belowground autotrophic respiration) exhibit significant positive trends over time ( $P=0.012$  for  $R_H:\text{GPP}_{\text{MTE}}$ ,  $P<0.01$  for all others; Fig. 2a) relative to GPP. These results are controlled, as above, for climate, land cover, partitioning method and disturbance. Grasslands exhibited much stronger  $R_S:\text{GPP}$  trends than forests for both the MODIS<sup>11</sup> and MTE<sup>10</sup> GPP datasets, perhaps because of their frequently high belowground carbon allocation.

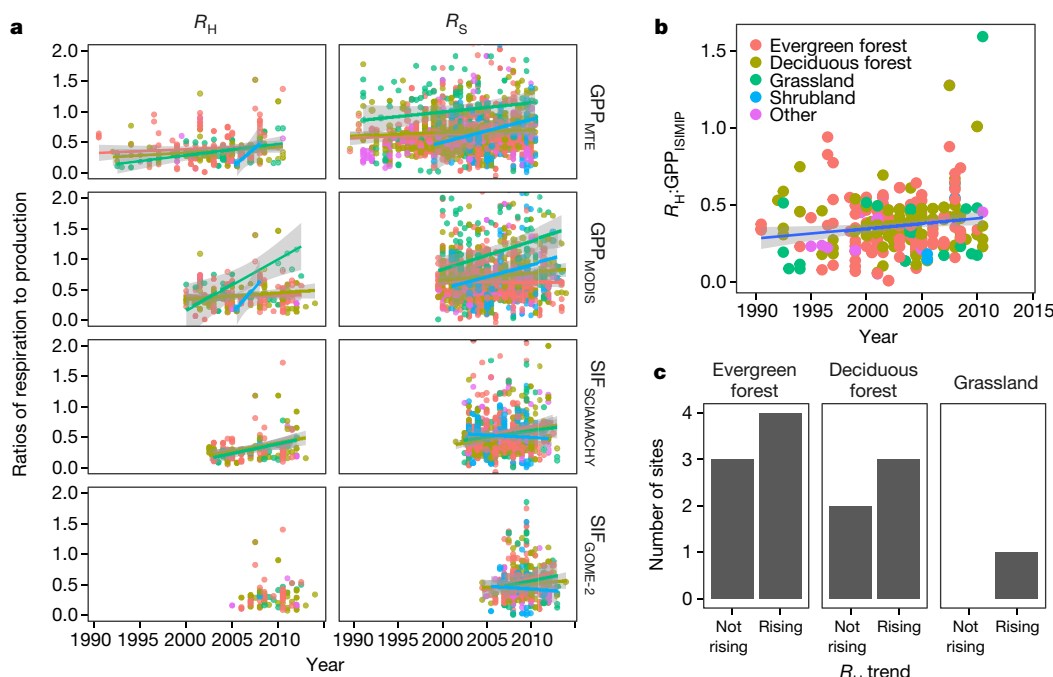
Solar-induced chlorophyll fluorescence (SIF) is correlated with GPP and provides an independent test of how  $R_H$  is related to carbon

assimilation over time. We examined the ratios of  $R_H$  and  $R_S$  to two global SIF data products (SCIAMACHY and GOME-2; see Methods). Both  $R_H$  and  $R_S$  exhibited temporal trends against the SCIAMACHY data after controlling for disturbance and measurement method ( $P<0.001$  for both; Fig. 2a). No  $R_H:\text{SIF}$  temporal trend was found using the GOME-2 SIF data, and  $R_S:\text{SIF}$  was only marginally significant ( $P=0.045$ ), but this is by far the shortest (2007–2014) of the datasets tested.

It is important to note that remotely sensed GPP and SIF estimates may not fully capture GPP increases owing to, for example, CO<sub>2</sub> fertilization<sup>22</sup>. The results above are, however, robust to such potential ‘missed’ GPP, even if one assumes a high rate of CO<sub>2</sub>-driven GPP increase completely missed by satellite-based products (Extended Data Figs. 4 and 5). We also found a significant ( $P=0.008$ ,  $n=263$ ) temporal  $R_H:\text{GPP}$  trend using GPP from a wide range of global models<sup>23</sup> that include CO<sub>2</sub> fertilization mechanisms (Fig. 2b), again controlling for the previously mentioned variables. This underscores the robustness of the trends shown in Fig. 2a.

A second challenge to the above analysis is the large spatial mismatch between remotely sensed GPP and SIF data (over  $10^9 \text{ m}^2$ ) versus  $R_H$  and  $R_S$  measurements (about  $1 \text{ m}^2$ ). To address this, we used eddy-covariance C flux data reported in the FLUXNET2015 database to examine temporal changes in co-located ecosystem respiration and production. Nighttime net ecosystem exchange (NEE<sub>night</sub>) is generally dominated<sup>24</sup> by  $R_S$ . Consequently, NEE<sub>night</sub> might increase relative to GPP over time, if  $R_H$  and thus  $R_S$  are rising. We used the full ‘Tier 1’ dataset ( $n=1,162$ ) to test this expectation and found that the annual NEE<sub>night:</sub>GPP<sub>fluxnet</sub> ratio is significantly rising with time ( $P=0.002$ ). We also attempted to use FLUXNET data to identify GPP measurements made in the same study site and year as site-specific  $R_S$  measurements, but from a bootstrap analysis, concluded that the small size of this dataset was unlikely to be adequate for this purpose (Extended Data Figs. 7 and 8).

A third problem is that, as in many previous global syntheses, the above analyses combine time and space responses. For a final test,

**Fig. 2 | Changes in ratios of respiration to production over time.**

a, Changes in the ratio of respiration to GPP and SIF over time. Two respiration fluxes ( $R_H$  and  $R_S$ ), two GPP sources (the MTE and MODIS datasets), and two SIF sources (the SCIAMACHY and GOME-2 datasets) are shown. For clarity, several high-ratio points are cut off. Points and linear regression lines are coloured by land cover (see key in b); lines in panel imply that the overall temporal trend was significant in that panel. Grey shading shows 95% confidence intervals; residuals from these

models are shown in Extended Data Fig. 3. b, Changes in the ratio of field-measured  $R_H$  to GPP modelled by suite of land models<sup>23</sup> over time. The trend line shows the statistically significant ( $P<0.001$ ) positive temporal trend in  $R_H:\text{GPP}$  using the GPP of ISIMIP models (see Table 1) and accounting for climate, land cover, disturbance and so on. c, Site-specific  $R_H$  trends in managed, unmanaged and natural ecosystems. Linear trend (not rising, slope  $\leq 0$ , versus rising, slope  $>0$ ) of  $R_H$  for sites in the SRDB<sup>9</sup> reporting at least three annual  $R_H$  measurements over at least eight years.

**Table 2 | Evidence supporting a global rise in soil  $R_H$** 

Test	n	Temporal trend?	Land cover significant?
Increasing $R_H:R_S$	318	Yes	No
Increasing $R_H:GPP_{MTE}$	266	Yes	No
Increasing $R_S:GPP_{MTE}$	1,622	Yes*	Yes
Increasing $R_H:GPP_{MODIS}$	251	Yes	Yes
Increasing $R_S:GPP_{MODIS}$	1,256	Yes	Yes
Increasing $R_H:SIF_{SCIA}$	183	Yes	No
Increasing $R_S:SIF_{SCIA}$	879	Yes	No
Increasing $R_H:SIF_{GOME-2}$	90	No	No
Increasing $R_S:SIF_{GOME-2}$	402	Yes	No
Increasing $R_S:GPP_{fluxnet}$	121	No	Yes
Increasing $NEE_{night}:GPP_{fluxnet}$	1,162	Yes	Yes
Increasing $R_H:GPP_{ISIMIP}$	263	Yes	No
$R_H$ climate response	332	N/A	No

Tests examined changes in ratios of  $R_H$  to  $R_S$ ;  $R_H$  and  $R_S$  to GPP and SIF;  $NEE_{night}$  to FLUXNET<sup>12</sup> GPP; ISIMIP<sup>23</sup> GPP; and the response of  $R_H$  to climate. Columns include number of observations (n), significance ( $P < 0.05$ ) of a 1989–2014 temporal trend after climate and other factors are accounted for in a linear regression, and whether the temporal trend was influenced by land cover (coniferous forest, deciduous forest, grassland, savannah, other). All temporal trends were also significant in a Theil–Sen robust regression unless otherwise noted with an asterisk.

we examined longitudinal, site-level  $R_H$  records from both managed and unmanaged ecosystems. There are only 13 sites in SRDB with such long-term records, and 8 of these exhibit rising  $R_H$  (Fig. 2c); when these data are pooled and controlled for climate, mean  $R_H$  also exhibits a significant ( $P < 0.001$ ) rising trend. This sample is very small and lies in a tighter climate change space than the main dataset (Extended Data Fig. 9), but the prevailing positive trend for a majority of sites is consistent with the analyses above given the site-specific diversity of factors controlling  $R_H$  responses to climate and atmospheric CO<sub>2</sub> changes. Several sensitivity analyses (see Methods) suggest that, because of their high variability and short record length, individual sites in both FLUXNET and SRDB remain unable to reliably detect an increase in  $R_H$ ; the signal is only slowly emerging from the noise, even for sites with multi-decadal records and across ecosystem types (Extended Data Fig. 6).

In summary, we have shown that multiple independent results (Table 2) converge to point towards a consistent finding of rising global  $R_H$ . This could be explained by at least two mechanisms, which are not mutually exclusive.

First, increased  $R_H$  might be temporarily fuelled by shifts in SOC forms and availability, and thus increased substrates for SOC mineralization, with little or no change in total SOC<sup>8</sup>. For example, eddy-covariance measurements from >10-yr FLUXNET sites indicate<sup>25,26</sup> that increases in GPP are outpacing concurrent rises in ecosystem respiration, resulting in greater ecosystem C uptake and detritus production, and thus greater bioavailable C for microbial metabolism. Highly productive grasslands and deciduous forests might be expected to respond more quickly to abiotic drivers<sup>27</sup>, and more slowly decomposing evergreen litter may even inhibit microbial activities<sup>28</sup>, together potentially explaining the trends shown in Fig. 2. This would be consistent with a 2015 inferred (as a residual, not measured) land sink of  $1.9 \pm 0.9$  Pg C yr<sup>-1</sup> (ref. <sup>29</sup>), but such a substrate-driven mechanism is not likely to be permanent, given the imbalance between soil C inputs and outputs (Fig. 2a). The C mass balance reported by FLUXNET sites exhibiting increased GPP and litter production<sup>25,26</sup> also suggests that new substrate inputs are not rising fast enough to keep up with increasing  $R_H$ .

A second and more tenable possibility is that rising  $R_H$  reflects enhanced SOC mineralization driven by climate changes, in particular rising global temperatures. If (as we calculate) global  $R_H$  has risen by approximately 1.2% over 25 years, against a mean air temperature change of +0.7 °C, this would be broadly consistent with warming experiment syntheses<sup>13–16</sup>. Assuming that rising  $R_H$  does in fact reflect SOC losses, this raises a consistency problem with estimated increases

in the terrestrial C sink<sup>29</sup>. It also poses a methodological challenge: small changes in  $R_H$  and SOC are difficult and perhaps impossible (see Methods) to detect at individual sites, even those with a decade or more of data, but will add up to substantial losses at the global scale.

A number of limitations should be noted. The SRDB (as well as most Earth-observing networks such as FLUXNET) is dominated by data from Northern Hemisphere, upland sites, and there are relatively few data from high latitudes and tropics (about 14% of SRDB for each), relative to the large areas and carbon pools of these biomes. Some of the data are also not fully independent: for example,  $R_H$  is usually measured independently of  $R_S$ , but occasionally (3–5% of these data) it is estimated by subtraction of autotrophic respiration from  $R_S$ , introducing an autocorrelation. Finally, any observational analysis such as this infers causality, and thus it is necessary to maintain and expand long-term manipulative experiments<sup>13,17</sup>.

These results pose new scientific challenges and opportunities for model benchmarking, hypothesis generation and testing, ecological forecasting and experiments. Rigorously testing for global SOC changes will require improvements in measuring, reporting and verification protocols, as it is not currently possible to derive a time-variant SOC map from repeated inventories except in ‘Tier 3’ countries<sup>30</sup>. More open global datasets of SOC stocks and fluxes<sup>9</sup>, and more broadly distributed long-term ecological study sites with systematic and repeated  $R_S$ ,  $R_H$ , and SOC measurements will help to test this finding of rising global  $R_H$  in the face of a seemingly stable or increasing terrestrial C sink.

## Online content

Any Methods, including any statements of data availability and Nature Research reporting summaries, along with any additional references and Source Data files, are available in the online version of the paper at <https://doi.org/10.1038/s41586-018-0358-x>.

Received: 30 March 2017; Accepted: 11 June 2018;

Published online 1 August 2018.

- Köchy, M., Hiederer, R. & Freibauer, A. Global distribution of soil organic carbon—Part 1: Masses and frequency distributions of SOC stocks for the tropics, permafrost regions, wetlands, and the world. *Soil* **1**, 351–365 (2015).
- Scharlemann, J. P. W., Tanner, E. V. J., Hiederer, R. & Kapos, V. Global soil carbon: understanding and managing the largest terrestrial carbon pool. *Carbon Manag.* **5**, 81–91 (2014).
- Bond-Lamberty, B. & Thomson, A. M. Temperature-associated increases in the global soil respiration record. *Nature* **464**, 579–582 (2010).
- Hashimoto, S. et al. Global spatiotemporal distribution of soil respiration modeled using a global database. *Biogeosciences* **12**, 4121–4132 (2015).
- Friedlingstein, P. et al. Uncertainties in CMIP5 climate projections due to carbon cycle feedbacks. *J. Clim.* **27**, 511–526 (2014).
- Zhou, T., Phi, P., Hui, D. & Luo, Y. Global pattern of temperature sensitivity of soil heterotrophic respiration ( $Q_{10}$ ) and its implications for carbon-climate feedback. *J. Geophys. Res. Biogeosci.* **114**, G02016 (2009).
- Trumbore, S. E. & Czimczik, C. I. An uncertain future for soil carbon. *Science* **321**, 1455–1456 (2008).
- Giardina, C. P., Litton, C. M., Crow, S. E. & Asner, G. P. Warming-related increases in soil CO<sub>2</sub> efflux are explained by increased below-ground carbon flux. *Nat. Clim. Change* **4**, 822–827 (2014).
- Bond-Lamberty, B. & Thomson, A. M. A global database of soil respiration data. *Biogeosciences* **7**, 1915–1926 (2010).
- Jung, M. et al. Global patterns of land-atmosphere fluxes of carbon dioxide, latent heat, and sensible heat derived from eddy covariance, satellite, and meteorological observations. *J. Geophys. Res. Biogeosci.* **116**, G00J07 (2011).
- Zhao, M., Heinsch, F. A., Nemani, R. R. & Running, S. W. Improvements of the MODIS terrestrial gross and net primary production global data set. *Remote Sens. Environ.* **95**, 164–176 (2005).
- Baldocchi, D. D. ‘Breathing’ of the terrestrial biosphere: lessons learned from a global network of carbon dioxide flux measurement systems. *Aust. J. Bot.* **56**, 1–26 (2008).
- Crowther, T. W. et al. Quantifying global soil carbon losses in response to warming. *Nature* **540**, 104–108 (2016).
- Lu, M. et al. Responses of ecosystem carbon cycle to experimental warming: a meta-analysis. *Ecology* **94**, 726–738 (2013).
- Wang, X. et al. Soil respiration under climate warming: differential response of heterotrophic and autotrophic respiration. *Glob. Change Biol.* **20**, 3229–3237 (2014).
- Zhou, L. et al. Interactive effects of global change factors on soil respiration and its components: a meta-analysis. *Glob. Change Biol.* **22**, 3157–3169 (2016).
- Melillo, J. M. et al. Long-term pattern and magnitude of soil carbon feedback to the climate system in a warming world. *Science* **358**, 101–105 (2017).

18. Bond-Lamberty, B., Wang, C. & Gower, S. T. A global relationship between the heterotrophic and autotrophic components of soil respiration? *Glob. Change Biol.* **10**, 1756–1766 (2004).
19. Davidson, E. A. & Janssens, I. A. Temperature sensitivity of soil carbon decomposition and feedbacks to climate change. *Nature* **440**, 165–173 (2006).
20. Hursh, A. et al. The sensitivity of soil respiration to soil temperature, moisture, and carbon supply at the global scale. *Glob. Change Biol.* **23**, 2090–2103 (2017).
21. Vargas, R. et al. On the multi-temporal correlation between photosynthesis and soil CO<sub>2</sub> efflux: reconciling lags and observations. *New Phytol.* **191**, 1006–1017 (2011).
22. Anav, A. et al. Spatiotemporal patterns of terrestrial gross primary production: a review. *Rev. Geophys.* **53**, 2015RG000483 (2015).
23. Warszawski, L. et al. The Inter-Sectoral Impact Model Intercomparison Project (ISI-MIP): project framework. *Proc. Natl Acad. Sci. USA* **111**, 3228–3232 (2014).
24. Falge, E. et al. Seasonality of ecosystem respiration and gross primary production as derived from FLUXNET measurements. *Agric. For. Meteorol.* **113**, 53–74 (2002).
25. Pilegaard, K., Ibrom, A., Courtney, M. S., Hummelshøj, P. & Jensen, N. O. Increasing net CO<sub>2</sub> uptake by a Danish beech forest during the period from 1996 to 2009. *Agric. For. Meteorol.* **151**, 934–946 (2011).
26. Urbanski, S. P. et al. Factors controlling CO<sub>2</sub> exchange on timescales from hourly to decadal at Harvard Forest. *J. Geophys. Res.* **112**, G02020 (2007).
27. Keenan, T. F. et al. Increase in forest water-use efficiency as atmospheric carbon dioxide concentrations rise. *Nature* **499**, 324–327 (2013).
28. Adamczyk, S., Adamczyk, B., Kitunen, V. & Smolander, A. Monoterpenes and higher terpenes may inhibit enzyme activities in boreal forest soil. *Soil Biol. Biochem.* **87**, 59–66 (2015).
29. Le Quéré, C. et al. Global carbon budget 2016. *Earth Syst. Sci. Data* **8**, 605–649 (2016).
30. Vargas, R., Paz, F. & de Jong, B. Quantification of forest degradation and belowground carbon dynamics: ongoing challenges for monitoring, reporting and verification activities for REDD+. *Carbon Manag.* **4**, 579–582 (2013).

**Acknowledgements** We are indebted to the thousands of researchers who measured and published the data collected here. This work used eddy-covariance data acquired and shared by the FLUXNET community (see Methods). This research was supported by the US Department of Energy, Office of Science, Biological and Environmental Research as part of the Terrestrial Ecosystem Sciences Program. The Pacific Northwest National Laboratory is operated for DOE by Battelle Memorial Institute under contract DE-AC05-76RL01830. R.V. acknowledges support from NASA-CMS (80NSSC18K0173) and USDA (2014-67003-22070). C.M.G. received additional support from the National Science Foundation Division of Environmental Biology, Award 1353908.

**Reviewer information** *Nature* thanks A. Konings, K. Ogle and the other anonymous reviewer(s) for their contribution to the peer review of this work.

**Author contributions** B.B.-L. conceived this study, and together with C.M.G. and R.V. designed the analysis. M.C. provided SIF data processing and expertise, and with V.L.B. furnished key insights. B.B.-L. wrote the manuscript in close collaboration with all authors.

**Competing interests** The authors declare no competing interests.

#### Additional information

**Extended data** is available for this paper at <https://doi.org/10.1038/s41586-018-0358-x>.

**Supplementary information** is available for this paper at <https://doi.org/10.1038/s41586-018-0358-x>.

**Reprints and permissions information** is available at <http://www.nature.com/reprints>.

**Correspondence and requests for materials** should be addressed to B.B.-L.

**Publisher's note:** Springer Nature remains neutral with regard to jurisdictional claims in published maps and institutional affiliations.

## METHODS

**Datasets.** This study used version v20170630a of the Global Soil Respiration Database (SRDB)<sup>9</sup>, downloaded 30 June 2017 from <https://github.com/bpbond/srdb>. We used only records in the SRDB from studies that (i) reported annual  $R_H$  and/or  $R_S$ ; (ii) had spatial (longitude and latitude) and temporal (measurement years) information; (iii) took place in natural or unmanaged ecosystems; (iv) had no experimental manipulation; and (v) used infrared gas analysers or gas chromatography (as opposed to for example, soda lime measurements that may underestimate CO<sub>2</sub> fluxes).

In general, the SRDB is oriented to seasonal to annual  $R_S$  data, and focuses on spatial breadth (a large number of sites around the world) rather than temporal detail (it does not attempt to capture continuous  $R_S$  measurements, for example). The annual fluxes used here occasionally come from continuous year-round measurements, but more often are computed by authors from interpolated manual measurements (mean measurement separation, 21 days; mean annual coverage, 89%). Such interpolation generally produces robust annual flux estimates<sup>31,32</sup>. Each site (that is, each unique longitude/latitude/ecosystem type combination) has on average 1.8–2.0 years of data, although a few have longer available records (see below).

These data ( $n = 334$  for  $R_H$  and  $n = 1,852$  for  $R_S$ ) were then spatially and temporally matched with a variety of ancillary datasets using the R ‘raster’ package version 2.5.8. Air temperature, precipitation and potential evapotranspiration came from the CRUTEM4 (Climatic Research Unit, University of East Anglia) climate data<sup>33</sup> downloaded 5 January 2017 from <http://www.cru.uea.ac.uk/data>. Because precipitation has higher uncertainty than temperature, and is only indirectly linked with the soil moisture that directly affects soil respiratory metabolism, we also examined the ESA Soil Moisture Climate Change Initiative (CCI) ‘Combined’ dataset, Version 0.2.2, downloaded 6 June 2017 from [http://data.ceda.ac.uk/neodc/esacci/soil\\_moisture/data/daily\\_files/COMBINED/v02.2/](http://data.ceda.ac.uk/neodc/esacci/soil_moisture/data/daily_files/COMBINED/v02.2/). Using these data instead of the CRU precipitation data did not change the overall results, but the ESA-CCI dataset has poor or no coverage in cloudy tropical regions (see ref.<sup>34</sup> for example and also <http://www.esa-soilmoisture-cci.org/node/93>), and when linked with the SRDB data under analysis here, 8% of data lacked soil moisture values, versus 5 (0.1%) lacking precipitation. We thus proceeded using precipitation only.

The bulk density and soil organic C content variables of the SoilGrids 1 km dataset<sup>35</sup> were downloaded on 8 January 2017 from <https://soilgrids.com> and used for a simple computation of 1 m SOC stock (as bulk density times C concentration). The geographic location of a few (around 10) soil respiration observations was missing in the SoilGrids dataset, and for these we substituted biome- and ecosystem-specific median values.

We used two global GPP datasets: the 1982–2011 MTE<sup>10</sup> GPP dataset, downloaded on 5 January 2017 from <https://www.bgc-jena.mpg.de/bgi/index.php/Services/Overview>, and the 2000–2015 MODIS GPP dataset<sup>11</sup> downloaded on 6 January 2017 from <http://www.ntsg.umt.edu/project/modis/mod17.php>. GPP data were used instead of NPP data because of the higher errors in the latter<sup>10,36</sup> due to uncertainties surrounding autotrophic respiration fluxes. We also extracted grid-cell-specific mean GPP from outputs of 8 global models in the ISIMIP<sup>23</sup> project, which uses community-agreed sets of scenarios with standardized climate variables and socio-economic projections.

For a more site-specific measure of GPP and C exchange, ‘Tier 1’ FLUXNET2015 data were downloaded on 30 January 2017 from <http://fluxnet.fluxdata.org/data/fluxnet2015-dataset/> and filtered for quality (NEE\_VUT\_REF\_QC  $\geq 0.5$ ). FLUXNET GPP was linked to a given  $R_S$  and/or  $R_H$  measurement if both measurements occurred within 5 km, in the same ecosystem type, and in the same year.

This work used eddy-covariance data acquired and shared by the FLUXNET community, including these networks: AmeriFlux, AfriFlux, AsiaFlux, CarboAfrica, CarboEuropeIP, CarboItaly, CarboMont, ChinaFlux, Fluxnet-Canada, GreenGrass, ICOS, KoFlux, LBA, NECC, OzFlux-TERN, TCOS-Siberia and USCCC. The ERA-Interim reanalysis data are provided by ECMWF and processed by LSCE. The FLUXNET eddy-covariance data processing and harmonization was carried out by the European Fluxes Database Cluster, AmeriFlux Management Project, and Fluxdata project of FLUXNET, with the support of CDIAC and ICOS Ecosystem Thematic Center, and the OzFlux, ChinaFlux and AsiaFlux offices. Data collected by Beringer in the OzFlux network was funded under an ARC FT (FT1110602). Specific FLUXNET sites and years used can be found in the Supplementary Information.

Finally, we used the global Solar-Induced chlorophyll Fluorescence (SIF) dataset from the Global Ozone Monitoring Experiment-2 (GOME-2) instrument onboard the MetOp-A platform and the SCanning Imaging Absorption spectroMeter for Atmospheric CHartographY (SCIAMACHY). This chlorophyll fluorescence signal is strongly linked with GPP<sup>37</sup> (although the ratio of SIF to GPP varies by land cover, and thus the SIF analysis is unable to capture changes in GPP due to land cover change). The monthly mean quality-filtered and gridded GOME-2 and SCIAMACHY SIF data (that is, SIF<sub>GOME-2</sub> and SIF<sub>SCIAMACHY</sub>) were used to reduce

the high data noise. The gridded GOME-2 data<sup>38</sup> is available at 0.5° resolution from 2007 to 2015, and SCIAMACHY<sup>39</sup> is at 1° from 2003 to 2011. These two datasets are so far the longest global SIF records. Both are publicly available at <ftp://ftp.gfz-potsdam.de/home/mefe/GlobFluo/>. For convenience in visualizing temporal changes in  $R_H$ :GPP and  $R_H$ :SIF ratios, SIF data were rescaled to the range of GPP (0–3,500 g C m<sup>-2</sup> yr<sup>-1</sup>) in plots.

In general, our analysis assumed the following basic relationships<sup>40</sup> between various carbon cycle fluxes:

Total soil respiration is the sum of its (belowground) autotrophic and heterotrophic components:

$$R_S = R_{A(\text{below})} + R_H$$

Autotrophic respiration is comprised of above- and belowground components:

$$R_A = R_{A(\text{above})} + R_{A(\text{below})}$$

NPP is the balance of GPP and autotrophic respiration:

$$\text{NPP} = \text{GPP} - R_A$$

In the absence of disturbance, NEE is equivalent to NPP minus  $R_H$ :

$$\text{NEE} \approx \text{NPP} - R_H$$

**Statistical analysis.** Some data were excluded a priori (that is, before constructing the analysis). These included: (i) studies performed before 1989, roughly when infrared gas analysers began to be widely used; (ii) several extremely high MODIS GPP values ( $>10$  kg C m<sup>-2</sup> yr<sup>-1</sup>); (iii) 27 points with  $R_S$ :GPP<sub>fluxnet</sub>  $> 5$ .

We used linear regression, weighted by years of  $R_H$  or  $R_S$  observation, to examine changes over time in the ratios of  $R_H$ : $R_S$ ,  $R_H$ :GPP,  $R_S$ :GPP,  $R_H$ :SIF and  $R_S$ :SIF, as well as the influence of climate on  $R_H$ . For each analysis detailed in the text, a full model was fitted for the variable of interest (for example, of  $R_H$ : $R_S$ ) that controlled for recent disturbance (the SRDB ‘Stage’ field, aggrading or mature), temperature and precipitation normals, and land cover; year of study had a first-order interaction with all these independent variables. Land-cover groupings included deciduous forests,  $n = 782$ ; evergreen forests,  $n = 1,058$ ; grasslands,  $n = 270$ ; savannahs,  $n = 116$ ; and other,  $n = 321$ . Both MAP and its square (that is, MAT<sup>2</sup>) were included<sup>20</sup>. All models were examined for influential outliers and deviations from normality; no transformation of dependent variables was performed. Non-significant terms were then eliminated using a forward-and-back stepwise algorithm (using the R package ‘MASS’, version 7.3-47) based on the Akaike Information Criterion. Generally the text reports  $F$  statistics and  $P$  values from the analysis of variance (ANOVA) results of these linear models. A Theil–Sen estimator<sup>41</sup> was also computed for each temporal trend, independent of the linear regressions, using the ‘mblm’ R package version 0.12.

A linear model relating  $R_H$  to climate—annual air temperature (°C), precipitation (mm) and its square—to allow for a nonlinear response<sup>20</sup>, potential evapotranspiration, recent disturbance, and leaf habit—was fitted (adjusted  $R^2 = 0.25$ , RSE = 23.3 g C m<sup>-2</sup> yr<sup>-1</sup>) and used to estimate global  $R_H$ . Global fluxes were based on 1989–2014 HadCRUT<sup>43</sup> data and projected onto a 0.5° grid (grid area data downloaded from <http://eos-webster.sr.unh.edu/>).

About one-third of the SRDB  $R_S$  data have associated uncertainties (that is, an annual flux reported as  $X \pm Y$ ) due to measurement error, spatial variability, and so on. The mean coefficient of variability for these  $R_S$  errors was 15%, and the median coefficient of variability was 10%. We did not attempt to propagate these uncertainties through our analysis, given their variable origin and incomplete nature, but a more complete treatment of uncertainty<sup>42</sup> will be important for testing the robustness of our results in the future.

**Sensitivity analyses.** We performed a number of tests to assess the robustness of our findings. To test whether the findings in Fig. 1 were an artefact of the 1989–2014 period chosen, the model summarized in Table 1 was repeatedly fitted to the SRDB dataset, as filtered with various first and final year assumptions (that is, the earliest and latest measurement allowed). We found that these results were not sensitive to choice of first and last years unless the timespan of the data was dramatically shortened (by at least 50%; Extended Data Fig. 1).

In addition, because satellites probably miss some large fraction of climate-driven terrestrial GPP increases<sup>22</sup>, we examined the robustness of the results in Fig. 2a to this potential problem. First, we quantified the divergence between eddy covariance (FLUXNET) and remotely sensed GPP (Extended Data Fig. 4). Second, we asked how much GPP would satellites have to be missing to invalidate the GPP-respiration trends shown in Fig. 2a using a sensitivity analysis that assumed a very conservative (that is, high) GPP trend<sup>43,44</sup> of 0.5% yr<sup>-1</sup> and repeatedly re-fitted the regressions shown in Fig. 2a assuming that satellites missed 0%, 10%, 20%, ..., 100% of this gain (Extended Data Fig. 5). Third, grid-cell-specific mean GPP was extracted from outputs of 15 global models in the ISIMIP<sup>23,45</sup> project—which

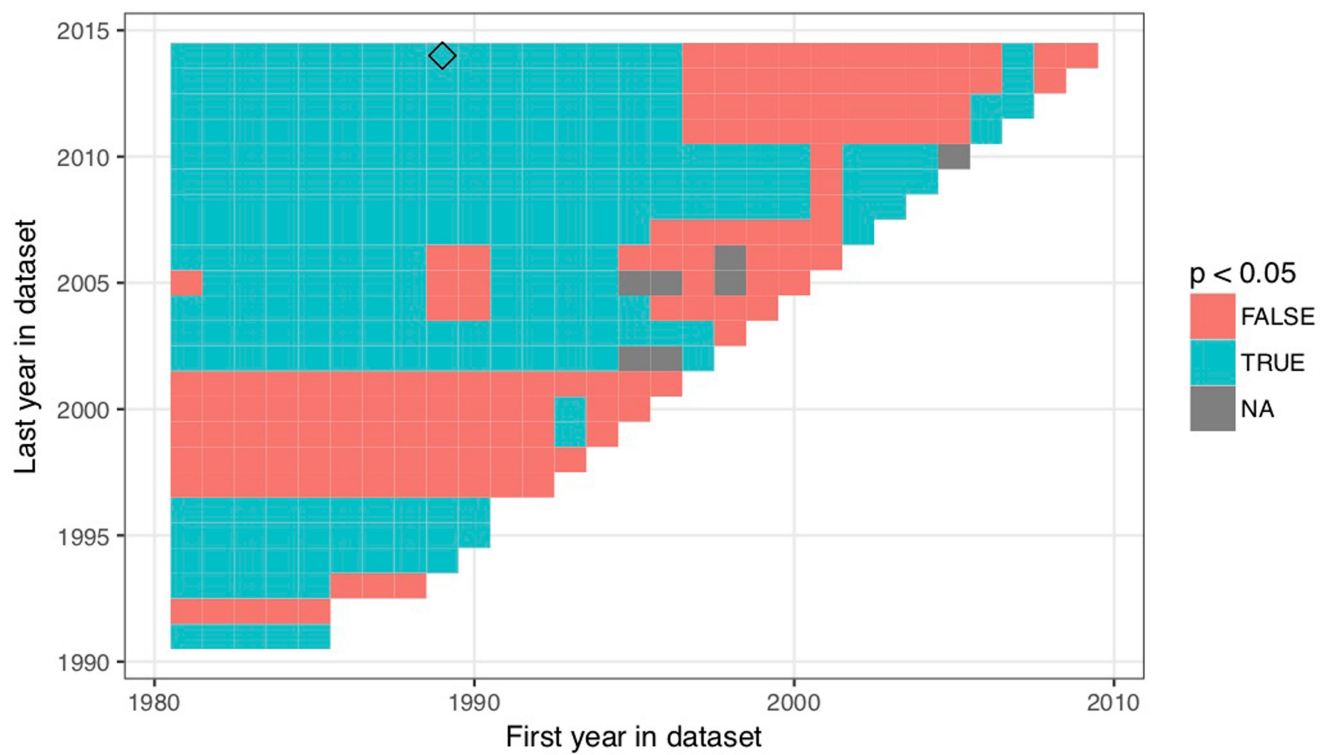
uses community-agreed sets of scenarios with standardized climate variables and socio-economic projections, and whose GPP models include CO<sub>2</sub> fertilization—and compared to observed  $R_H$  (Fig. 2B).

We also examined whether the inconsistency in longitudinal (site) results (Fig. 2c) fell within the range of what might naturally occur—that is, whether the variability was numerically consistent with the variability in global carbon flux datasets. To do so, we calculated the chance of observing a statistically significant  $R_H$  increase at some random location on Earth's surface over the last 25 years using a global gridded  $R_H$  dataset<sup>4</sup>, by testing for a significant temporal trend in each of its 57,048 terrestrial grid cells. We calculated this probability to be 26%: in other words, there would be only a 1-in-4 chance of observing a significant  $R_H$  increase even with a quarter-century of perfect data ('perfect' in the sense of no random measurement error, as would occur in reality), because the climate-driven  $R_H$  increase is small compared to interannual  $R_H$  variation. The probability of observing a statistically significant  $R_H$  increase using only the last 10 years' data, comparable to the record length of most of the 13 longitudinal sites (Fig. 2c), was only 5%. A parallel exercise was performed with the global GPP datasets and yielded similar results. We also compared the sites' location in climate change space with that of the overall Fig. 1 dataset (Extended Data Fig. 9).

Finally, we performed a bootstrap analysis to quantify whether the FLUXNET data subset (that included GPP measurements made in the same study site and year as site-specific  $R_S$  measurements in the SRDB) was adequate, as this was a small dataset ( $n = 106$  site-years, 19 sites) dominated by one site (Harvard Forest, with 56% of the available data). What was the likelihood that this dataset is simply too small to detect signals of rising  $R_H$ , given site-to-site variability in climate and carbon dynamics? To answer this we made different random draws from the original dataset, with 1,000 bootstrap draws per fraction of artificial no-trend data (Extended Data Figs. 7 and 8).

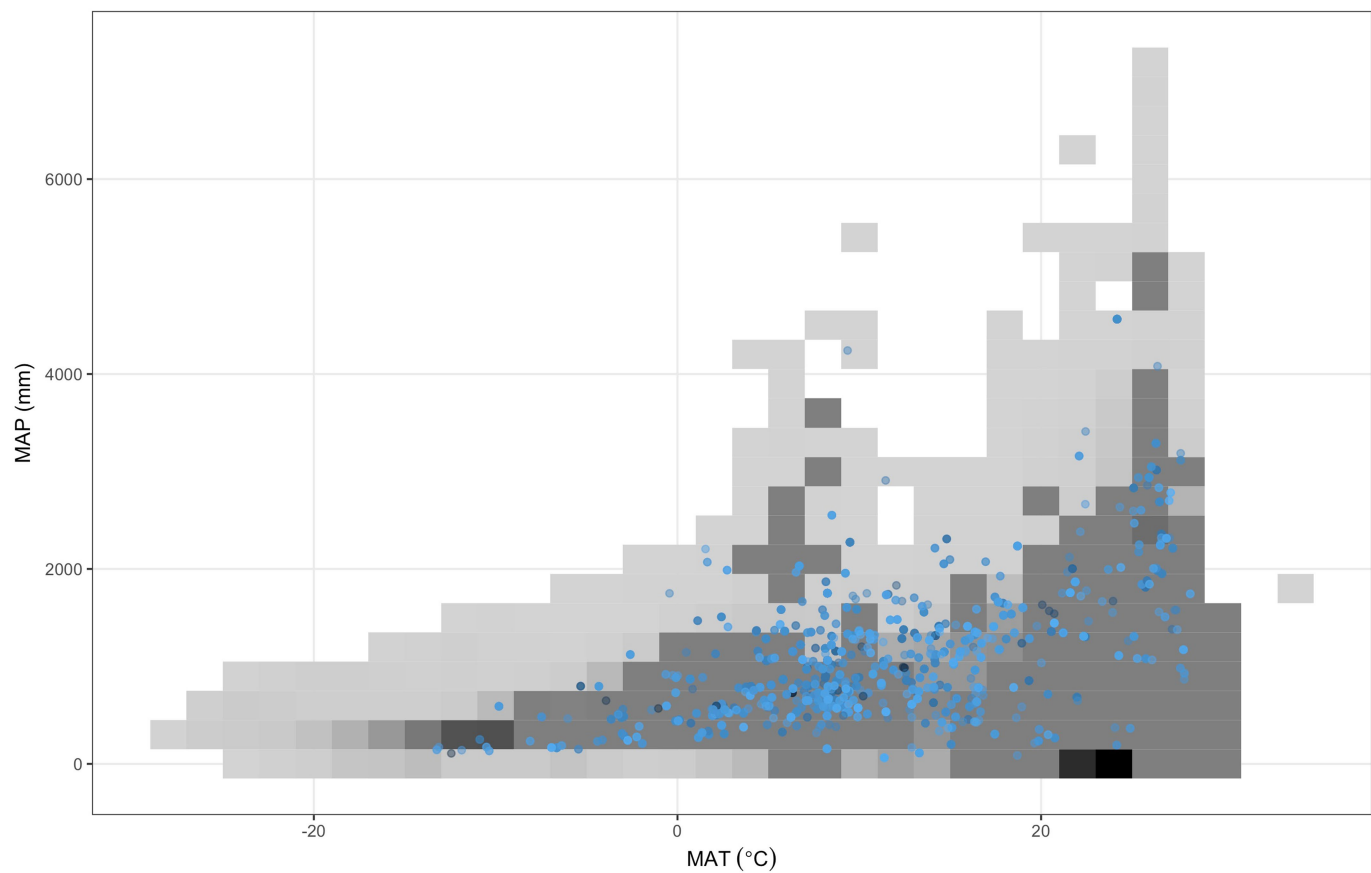
**Code and data availability.** The R language and environment for statistical computing<sup>46</sup> version 3.4.3 was used for all analyses. Code and data to reproduce all results are available at <https://github.com/bpbond/rh-changes>.

31. Wayson, C. A., Randolph, J. C., Hanson, P. J., Grimmond, C. S. B. & Schmid, H. P. Comparison of soil respiration methods in a mid-latitude deciduous forest. *Biogeochemistry* **80**, 173–189 (2006).
32. Reichstein, M. et al. Modeling temporal and large-scale spatial variability of soil respiration from soil water availability, temperature and vegetation productivity indices. *Glob. Biogeochem. Cycles* **17**, 1104 (2003).
33. Osborn, T. J. & Jones, P. D. The CRUTEM4 land-surface air temperature data set: construction, previous versions and dissemination via Google Earth. *Earth Syst. Sci. Data* **6**, 61–68 (2014).
34. Dorigo, W. et al. Evaluating global trends (1988–2010) in harmonized multi-satellite surface soil moisture. *Geophys. Res. Lett.* **39**, L18405 (2012).
35. Hengl, T. et al. SoilGrids1km — global soil information based on automated mapping. *PLoS ONE* **9**, e105992 (2014).
36. Ito, A. A historical meta-analysis of global terrestrial net primary productivity: Are estimates converging? *Glob. Change Biol.* **17**, 3161–3175 (2011).
37. Frankenberg, C. et al. New global observations of the terrestrial carbon cycle from GOSAT: patterns of plant fluorescence with gross primary productivity. *Geophys. Res. Lett.* **38**, L17706 (2011).
38. Joiner, J. et al. Global monitoring of terrestrial chlorophyll fluorescence from moderate-spectral-resolution near-infrared satellite measurements: methodology, simulations, and application to GOME-2. *Atmos. Meas. Tech.* **6**, 2803–2823 (2013).
39. Köhler, P., Guanter, L. & Joiner, J. A linear method for the retrieval of sun-induced chlorophyll fluorescence from GOME-2 and SCIAMACHY data. *Atmos. Meas. Tech.* **8**, 2589–2608 (2015).
40. Chapin, F. S. et al. Reconciling carbon-cycle concepts, terminology, and methods. *Ecosystems* **9**, 1041–1050 (2006).
41. Fernandes, R., Leblanc, S. G. Parametric (modified least squares) and non-parametric (Theil-Sen) linear regressions for predicting biophysical parameters in the presence of measurement errors. *Remote Sens. Environ.* **95**, 303–316 (2005).
42. Xu, M. & Shang, H. Contribution of soil respiration to the global carbon equation. *J. Plant Physiol.* **203**, 16–28 (2016).
43. Ito, A. et al. Photosynthetic productivity and its efficiencies in ISIMIP2a biome models: benchmarking for impact assessment studies. *Environ. Res. Lett.* **12**, 085001 (2017).
44. Kolby Smith, W. et al. Large divergence of satellite and Earth system model estimates of global terrestrial CO<sub>2</sub> fertilization. *Nat. Clim. Change* **6**, 306–310 (2016).
45. Rosenzweig, C. et al. Assessing inter-sectoral climate change risks: the role of ISIMIP. *Environ. Res. Lett.* **12**, 010301 (2017).
46. R Development Core Team. *R: A Language And Environment For Statistical Computing*. Version 3.3.3 (2017).

**Extended Data Fig. 1 | Effect of dataset temporal span on  $R_H:R_S$  trend.**

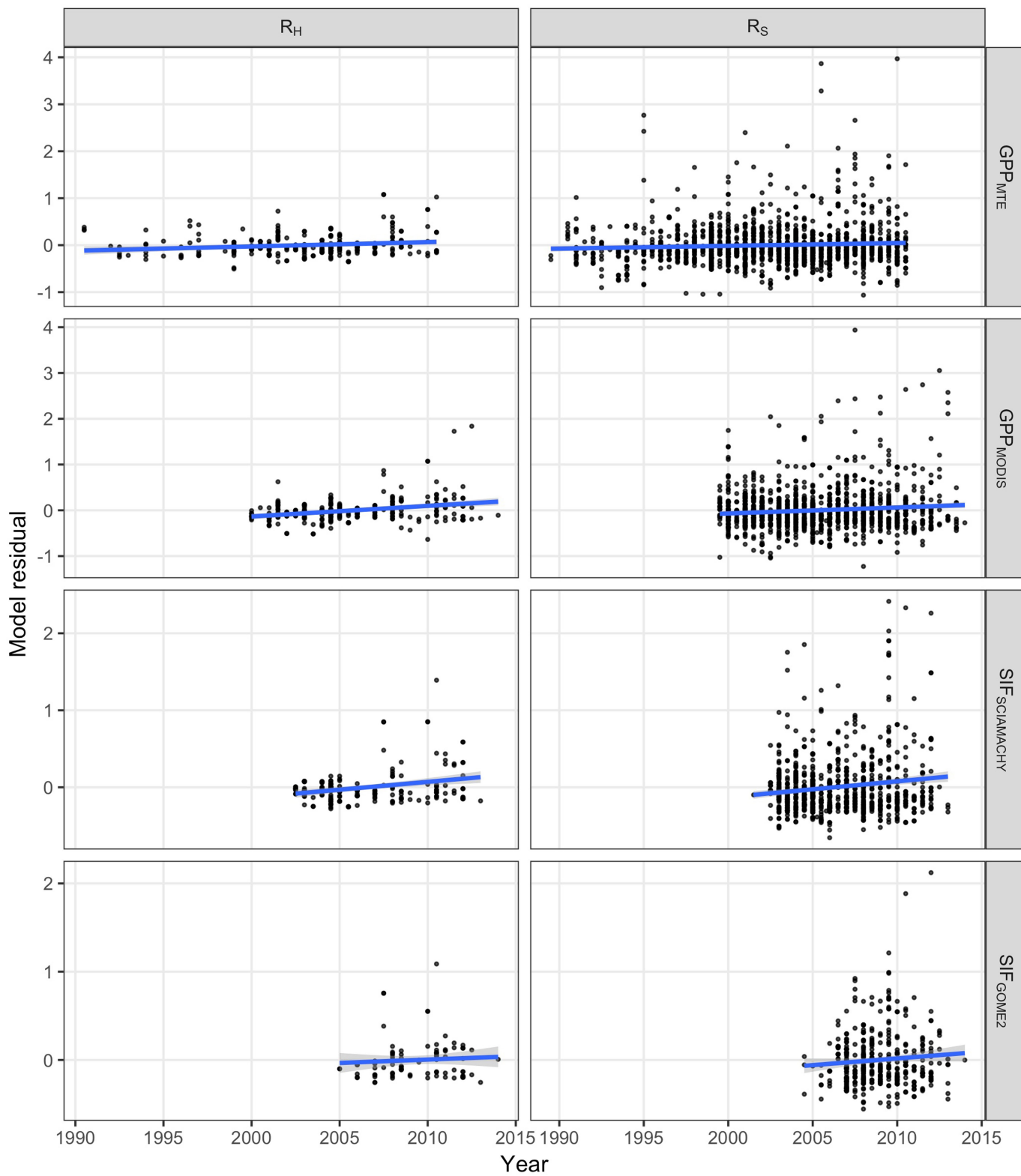
The model summarized in Table 1 was repeatedly fitted to the SRDB dataset, as filtered with various first and final year assumptions (that is, the earliest and latest measurement allowed, to test whether the results

were an artefact of the 1989–2014 period chosen, indicated by a black diamond in the figure). Colour shows the significance of the  $R_H:R_S$  temporal trend.



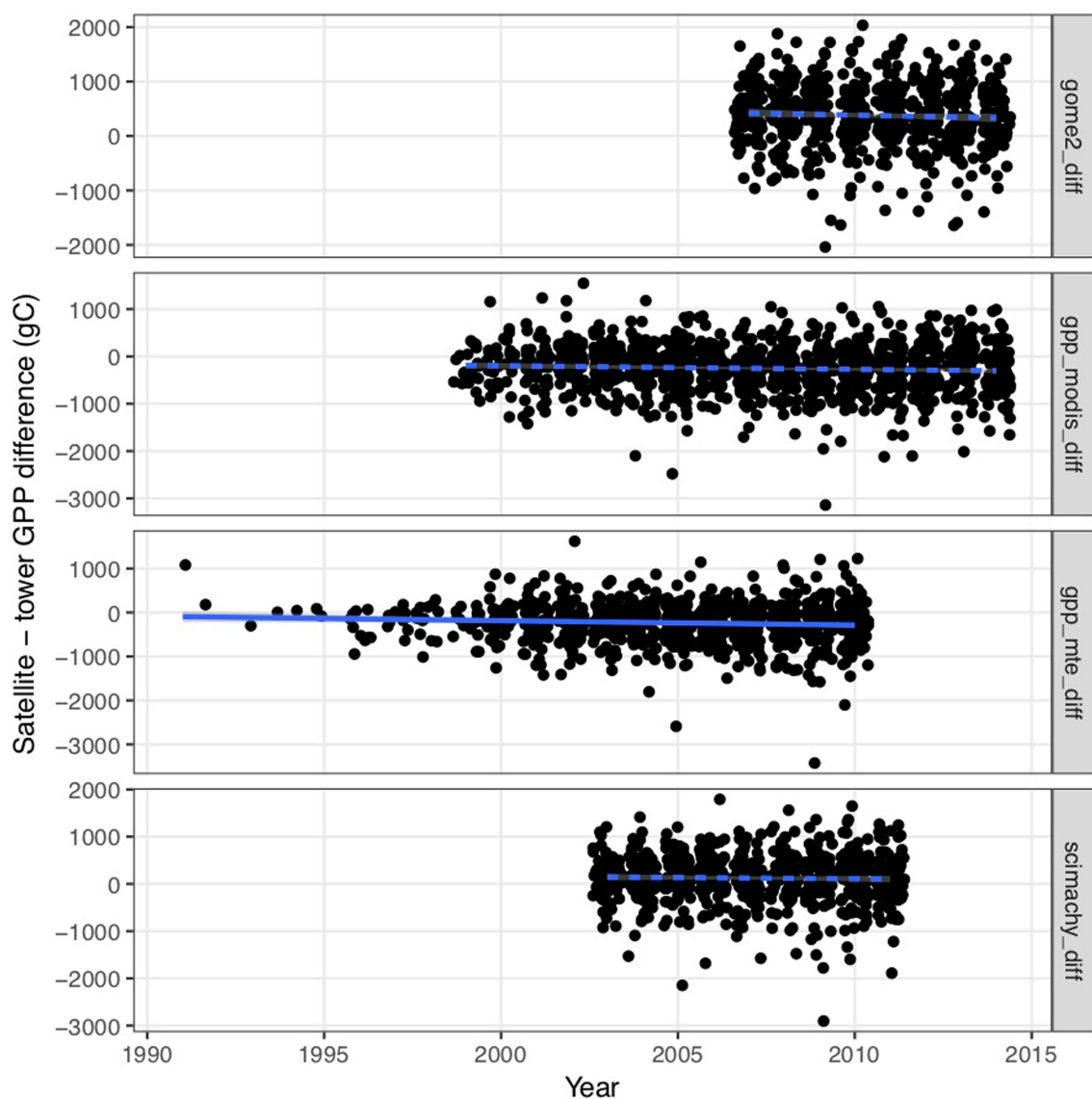
**Extended Data Fig. 2 | SRDB coverage in terrestrial climate space.** Blue dots show MAT and MAP of the entries in the database; lighter points indicate more recent data. Grey background indicates global climate

distribution in the HadCRUT4<sup>33</sup> data, with darker shades indicating more land area, for 1991–2010.



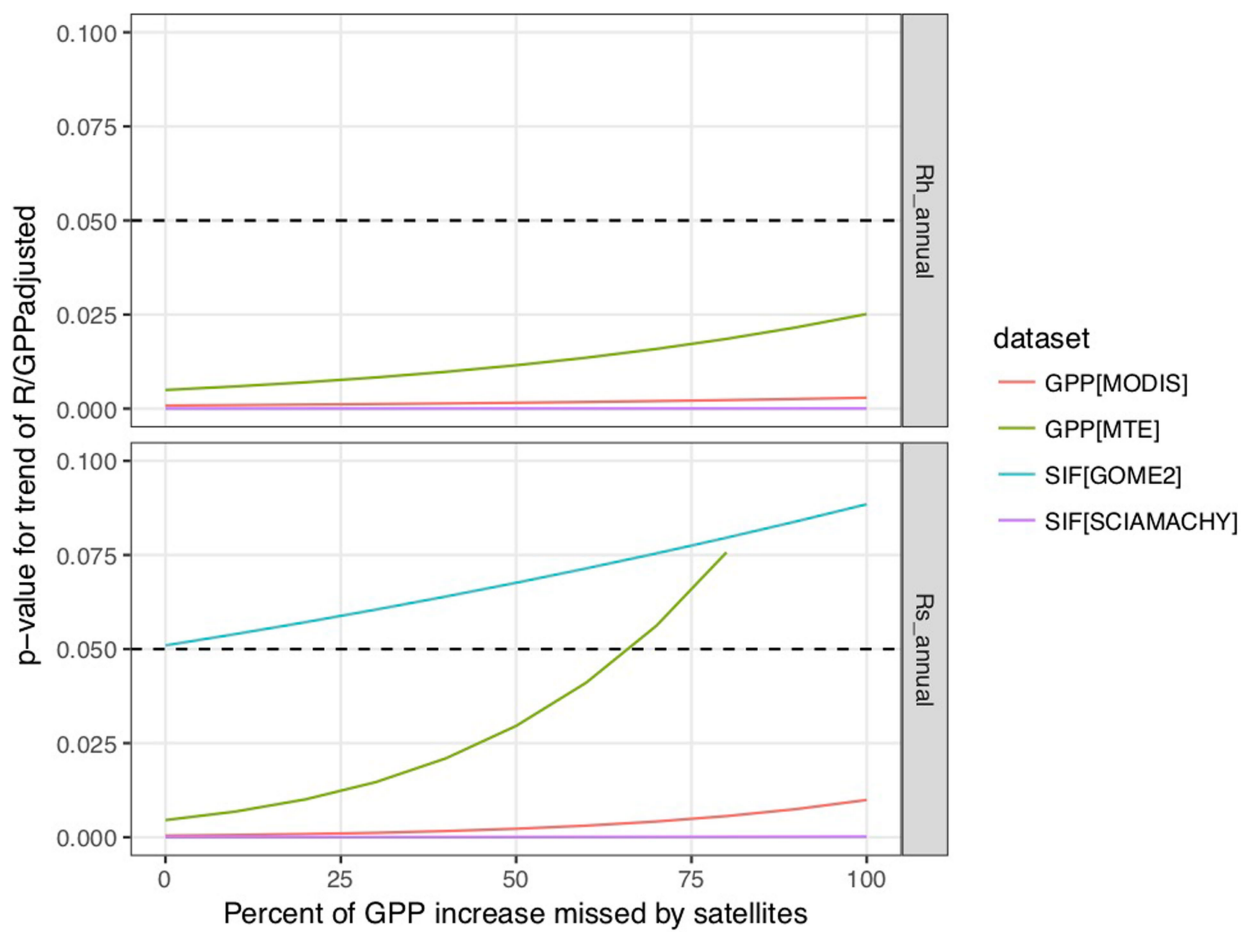
**Extended Data Fig. 3 | Respiration-to-production model residuals over time.** The model examines how the dependent variable—the ratio of respiration to GPP or SIF—is related to the independent variables: climate, land cover, disturbance and SOC content; for more details, see Methods. Two respiration fluxes ( $R_H$  and  $R_S$ ), two GPP sources (the statistically

upscaled MTE dataset, and the remotely sensed MODIS product), and two SIF sources (SCIAMACHY and GOME-2) are shown. Grey bands show 95% confidence intervals. Blue lines indicate least-squares trend, while grey bands show 95% confidence intervals.



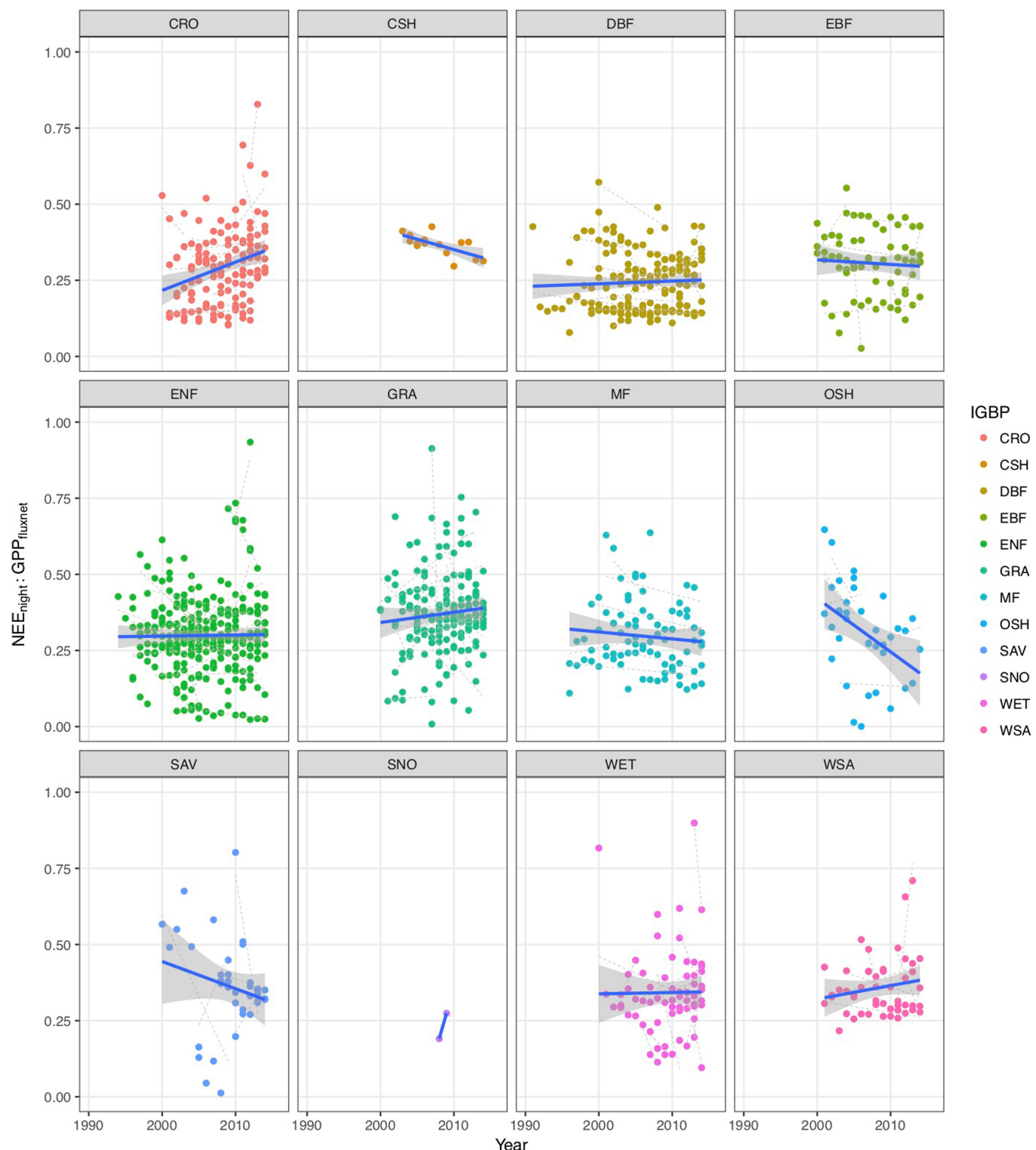
**Extended Data Fig. 4 | Difference between FLUXNET GPP and remotely sensed GPP and SIF over time.** Trends are not significant for the satellite data from GOME-2 SIF ( $P = 0.22$ ), MODIS GPP ( $P = 0.07$ ) or SCIMACHY SIF ( $P = 0.49$ ). Blue lines (solid line is statistically significant,

dashed line is non-significant) lines indicate least-squares trend. The temporal trend for MTE GPP decreases significantly ( $P = 0.02$ ) over time, that is, MTE GPP increasingly underpredicts GPP measured by eddy covariance tower.



**Extended Data Fig. 5 | Sensitivity analysis of how much GPP satellites would have to be missing to render the GPP-respiration trends shown in Fig. 2a non-significant.** We ran a sensitivity analysis that assumed a conservative (that is, high) GPP trend of  $0.5\% \text{ yr}^{-1}$ , and repeatedly re-fitted the Fig. 2a models assuming that satellites missed 0%, 10%, 20%,...100% of this gain. This figure plots the ‘missed’ percentage (x axis) versus the

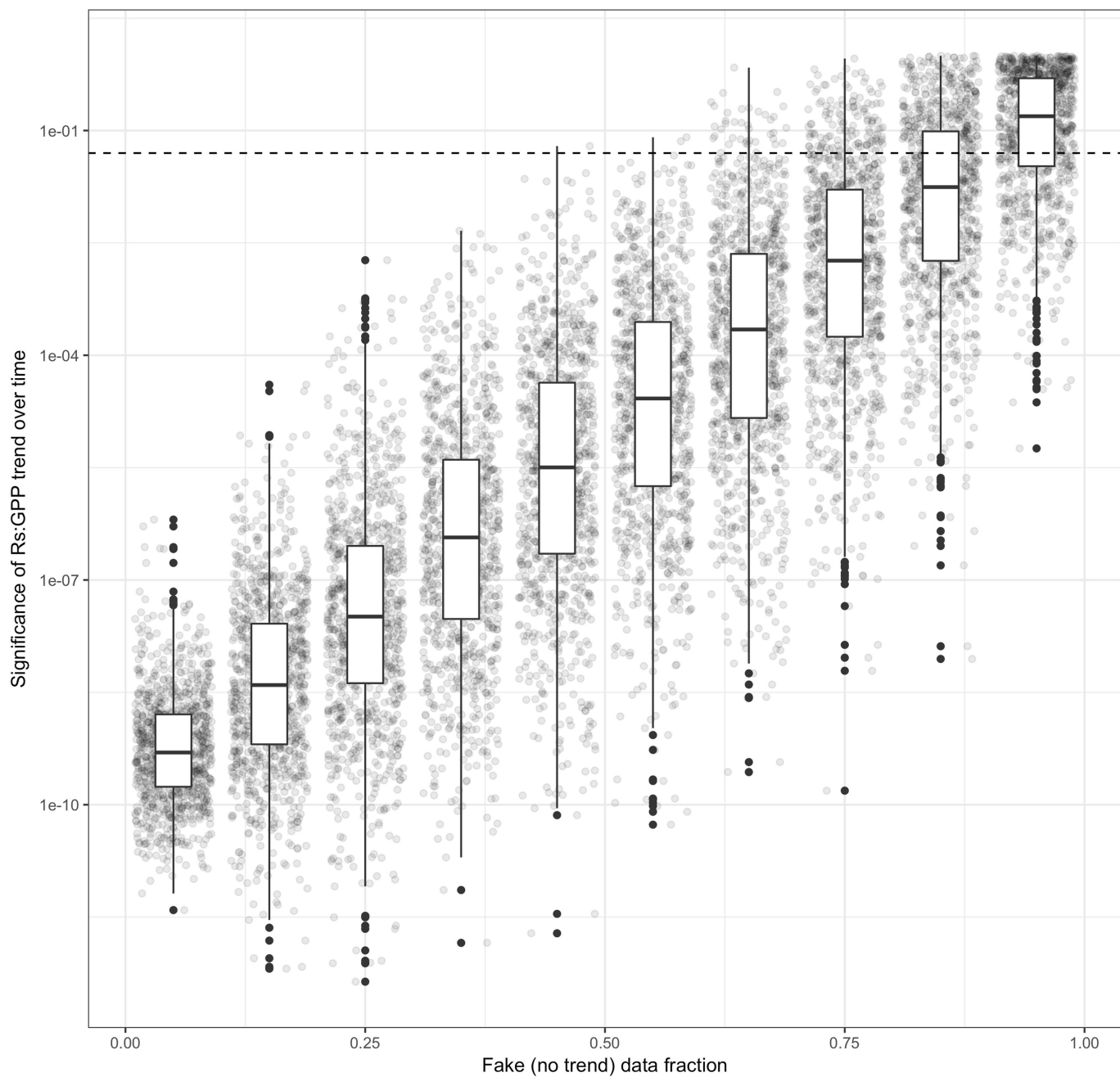
*P*-value of the linear regression (*y* axis) for each respiration flux ( $R_h$  and  $R_s$ ) and GPP or SIF data product (‘GPPadjusted’, that is, adjusted for the assumed ‘missed’ percentage). Even if satellites are missing 100% of this large assumed GPP increase, most of the temporal trends shown in Fig. 2a trends remain highly significant.



**Extended Data Fig. 6 | Ratio of NEE<sub>night</sub> to GPP in the FLUXNET 2015 ‘Tier 1’ dataset.** Panels show different International Geosphere-Biosphere Programme (IGBP) land cover type: crop (CRO), closed shrubland (CSH), deciduous broadleaf forest (DBF), evergreen broadleaf forest (EBF),

evergreen needleleaf forest (ENF), grassland (GRA), mixed forests (MF), open shrublands (OSH), herbaceous savannahs (SAV), snow and ice (SNO), wetlands (WET) and woody savannahs (WSA).

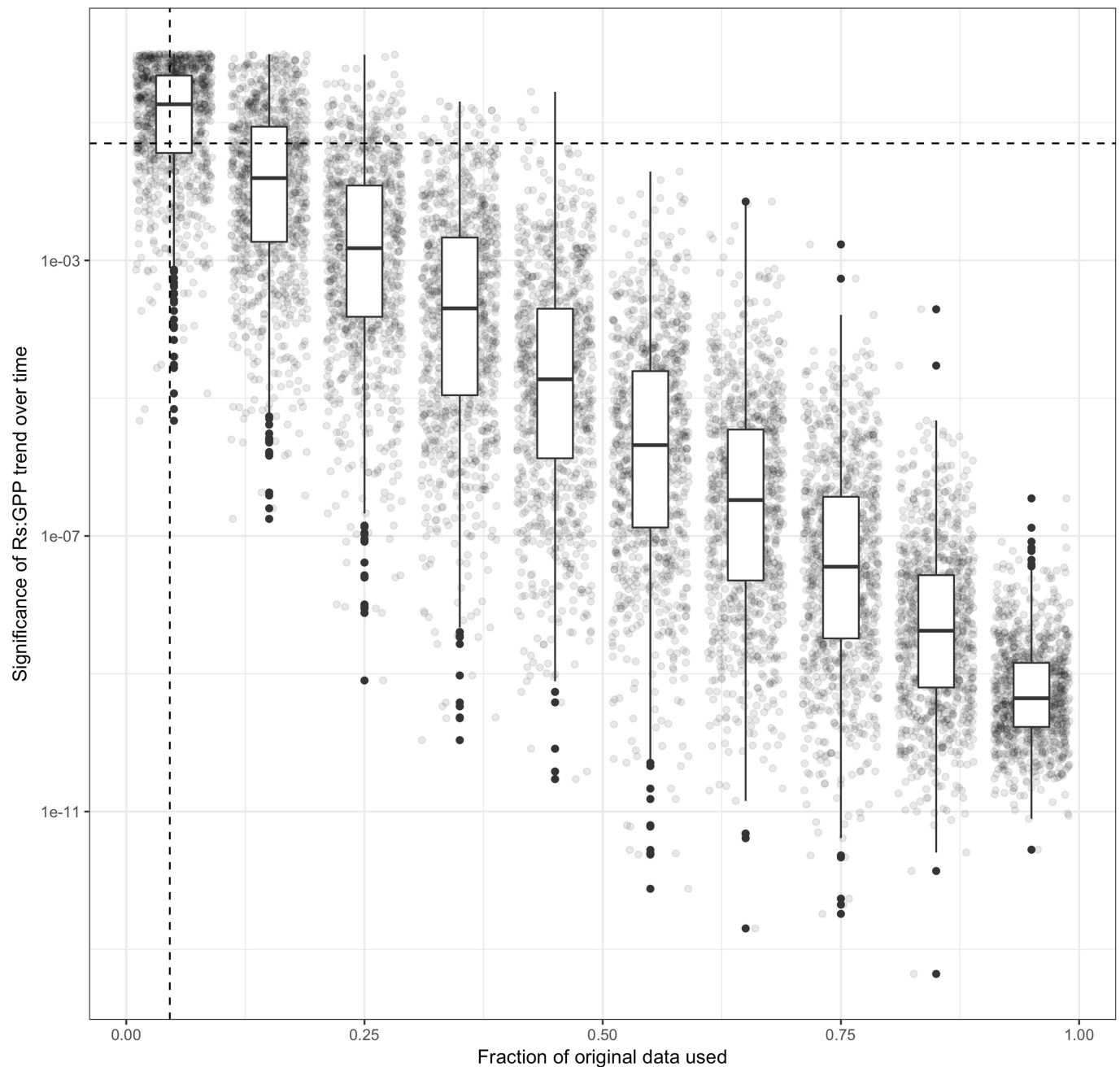
## s\_MODIS.GPP\_Rs\_annual N = 1000

**Extended Data Fig. 7 | Bootstrap analysis examining effect of ratio of significant to non-significant data on likelihood of observing a trend.**

What is the likelihood that the FLUXNET data subset (that included GPP measurements made in the same study site and year as site-specific RS measurements in the SRDB) is too small to detect signals of rising  $R_h$ , given site-to-site variability in climate and carbon dynamics? Each point is a different random draw from the original dataset, the comparison of  $R_s$  to

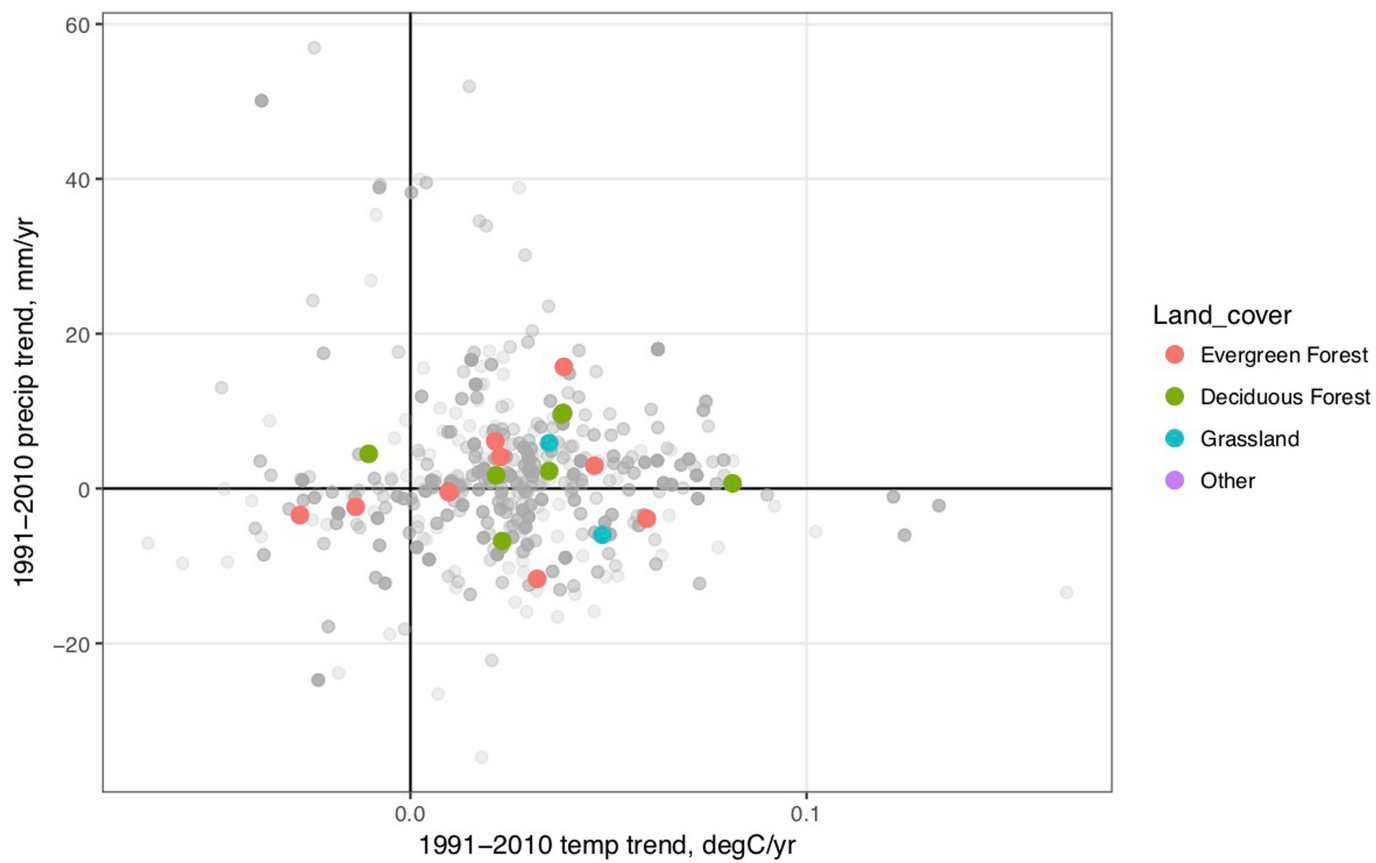
MODIS GPP, with 1,000 bootstrap draws per fraction of artificial no-trend data. The horizontal dashed line is  $P = 0.05$ . Note log scale (to base e, which R defaults to) of y axis. Boxplots visualize five summary statistics (the median, the first and third quartiles, and two whiskers; see [https://ggplot2.tidyverse.org/reference/geom\\_boxplot.html](https://ggplot2.tidyverse.org/reference/geom_boxplot.html)); points are semi-transparent to indicate data density at each point.

## s\_MODIS.GPP\_Rs\_annual N = 1000



**Extended Data Fig. 8 | Bootstrap analysis examining effect of dataset size on likelihood of observing a trend.** What is the likelihood that the  $n = 106$  FLUXNET dataset is too small to detect signals of rising  $R_h$ , given site-to-site variability in climate and carbon dynamics? Each point is a different random draw from the original dataset, the comparison of  $R_s$  to MODIS GPP, with 1,000 bootstrap draws per fraction of no-trend

data. The vertical dashed line shows the size of the original  $R_s$ :FLUXNET dataset, about 5% of the  $R_s$ :GPP<sub>MODIS</sub> data, while the horizontal line is  $P = 0.05$ . Note log scale (to base e) of y axis. Boxplots visualize five summary statistics (the median, the first and third quartiles, and two whiskers; see [https://ggplot2.tidyverse.org/reference/geom\\_boxplot.html](https://ggplot2.tidyverse.org/reference/geom_boxplot.html)); points are semi-transparent to indicate data density at each point.



**Extended Data Fig. 9 | Distribution of the longitudinal site data in climate change space relative to the main SRDB dataset.** The longitudinal data (Fig. 2c, coloured dots below) in climate change space (1991–2010 HadCRUT4 changes in air temperature and precipitation) are

shown over the distribution of the main dataset ( $n = 1,852$ , grey dots). The longitudinal data cover  $-0.03$  to  $+0.08 \text{ }^{\circ}\text{C yr}^{-1}$  and  $-12$  to  $+16 \text{ mm yr}^{-1}$ ; the main dataset covers a much broader climate change space of  $-0.07$  to  $+0.17 \text{ }^{\circ}\text{C yr}^{-1}$  and  $-35$  to  $+57 \text{ mm yr}^{-1}$ .

Extended Data Table 1 | Coefficients for general model<sup>18</sup> of relationship between  $R_S$  and  $R_H$ 

Coefficient	Estimate	Std. Error	t	P
(Intercept)	-27.771	7.653	-3.629	<0.001
$\log(R_S)$	0.867	0.033	26.044	<0.001
Year	0.014	0.004	3.653	<0.001

A model of form  $\ln(R_H) \approx \ln(R_S) * \text{Year}$  was fitted (following the protocol in ref. <sup>18</sup>) to the data shown in Fig. 1, with 'Year' being the numerical year of measurement. Coefficient name, value and standard error, t value and P value are shown. Model residual standard error = 0.335, adjusted  $R^2 = 0.698$ ,  $F_{2,317} = 396.6$ ,  $P < 0.001$ , AIC = 212.745.